



HAL
open science

Densification of MnSO₄ ceramics by Cool-SPS: Evidences for a complex sintering mechanism and magnetoelectric coupling

Thomas Hérisson de Beauvoir, F. Molinari, U-Chan Chung-Seu, Dominique Michau, Dominique Denux, Michaël Josse

► To cite this version:

Thomas Hérisson de Beauvoir, F. Molinari, U-Chan Chung-Seu, Dominique Michau, Dominique Denux, et al.. Densification of MnSO₄ ceramics by Cool-SPS: Evidences for a complex sintering mechanism and magnetoelectric coupling. *Journal of the European Ceramic Society*, 2018, 38 (11), pp.3867-3874. 10.1016/j.jeurceramsoc.2018.04.005 . hal-01815090

HAL Id: hal-01815090

<https://hal.science/hal-01815090>

Submitted on 13 Jun 2018

HAL is a multi-disciplinary open access archive for the deposit and dissemination of scientific research documents, whether they are published or not. The documents may come from teaching and research institutions in France or abroad, or from public or private research centers.

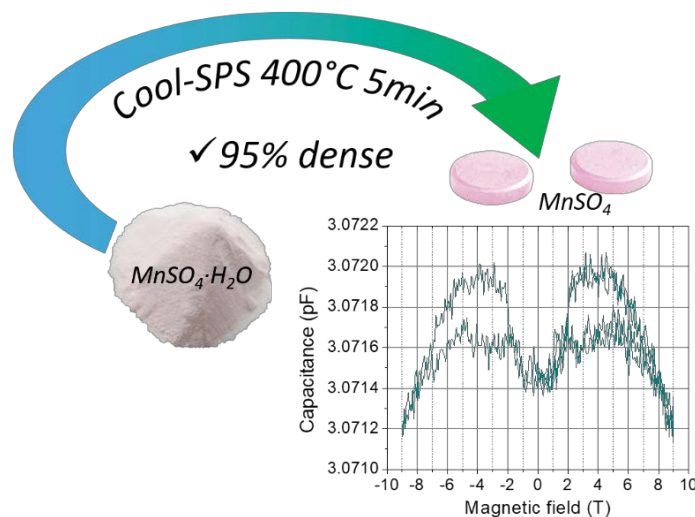
L'archive ouverte pluridisciplinaire **HAL**, est destinée au dépôt et à la diffusion de documents scientifiques de niveau recherche, publiés ou non, émanant des établissements d'enseignement et de recherche français ou étrangers, des laboratoires publics ou privés.

Densification of MnSO_4 ceramics by Cool-SPS: evidences for a complex sintering mechanism and magnetoelectric coupling

T. Herisson de Beauvoir, F. Molinari, U.C. Chung-Seu, D. Michau, D. Denux, M. Josse*

Abstract

Dense ceramics of MnSO_4 composition have been successfully densified at 400 °C in only 5 min under a uniaxial pressure of 400 MPa, using Spark Plasma Sintering technique. Since the stable form of MnSO_4 in ambient atmosphere is its hydrate $\text{MnSO}_4 \cdot \text{H}_2\text{O}$, crystallizing in a different space group, dehydration is required to reach a purely anhydrous phase. *In situ* dehydration during Spark Plasma Sintering allows to lower both sintering temperature and time. Applied pressure strongly influences dehydration step and therefore is a key parameter to tune densification, so far as to obtain a dense $\text{MnSO}_4 \cdot \text{H}_2\text{O}$ ceramic. The presence of a reversible phase transition to a $\beta\text{-MnSO}_4$ high temperature form seems to influence the dehydration temperature under pressure, and likely drives the sintering mechanisms. The high densification obtained, beyond 95 % of theoretical density, added to the preservation of the structural and physical properties of MnSO_4 after sintering allowed to perform reliable and reproducible measurements showing a dielectric anomaly associated to the magnetic transition, and the hysteretic behaviour of capacitance versus magnetic field, which is a clue for an intrinsic magnetoelectric coupling in MnSO_4 .



1. Introduction

Since their revival in the early 2000's [1–4], magnetoelectric (ME) and multiferroic (MF) materials have strongly aroused the interest of materials chemistry and physics communities. A large part of their work in this field is focused on the research of new MF and/or ME phases [5–7]. However, for single

phased materials, the scarcity of good candidates for multiferroism, all the more at room temperature, is well documented. This is, in part, due to the mutually excluding conditions for proper ferromagnetism and ferroelectricity, in transition metal oxides based on octahedral frameworks, among which most ferroelectric materials are found. This essentially prevents the appearance of multiferroic properties in a single phase material [1], the unique example of a ferroelectric ferromagnet being BiMnO_3 [8]. Starting from that point, Kimura postulated that improper ferroelectrics could be interesting candidates as ME materials, especially electronic ferroelectrics [2] such as those associated with a spiral magnetic structure [9]. In these magnetically driven ferroelectrics, a helical magnetic structure can, in specific conditions [10], break the inversion symmetry and generate an electric polarization along a specific direction, for example. Materials displaying such a behavior are classified as type II multiferroics [11], and among them is the prototypical MnWO_4 [12], which orders magnetically below 15K and displays a ferroelectric polarization four orders of magnitude smaller than classical ferroelectrics ($\text{BaTiO}_3 \sim 25 \mu\text{C}\cdot\text{cm}^{-2}$). However, research on type II multiferroics has been quite successful, unveiling the multiferroic properties of CuO at a rather high temperature ($T_c \sim 230\text{K}$) [13] and a polarization reaching $0,15 \mu\text{C}\cdot\text{cm}^{-2}$ in $\text{CaBaCo}_4\text{O}_7$ [14]. When looking for phases presenting such a helical magnetic structure, one can notice that the ferroelectric properties of some of the candidate phases have not been explored yet because of the difficulty to obtain dense ceramic samples by sintering. Usually, the thermal stability of these candidate phases is limited by low temperature decompositions, phase transitions... that prevent the use of conventional, pressureless sintering for their densification. However, the emergence of new sintering techniques opens opportunities to densify and study these thermodynamically fragile materials (referred to as *fragile materials* in the following). In the present work, we relied on the spark plasma sintering (SPS) technique for the densification of MnSO_4 which displays a helical magnetic structure at low temperature ($T_N = 11\text{K}$) [15] but decomposes at 780°C [16]. On the one hand, this relatively low decomposition temperature forbids any successful sintering by conventional solid-state technique (which we unsuccessfully attempted). On the other, SPS is a powerful technique that allows for rapid sintering of refractory materials at temperatures much lower than those requested for any conventional sintering, as for Al_2O_3 which can be sintered at 1050°C [17], while conventional sintering requires temperatures as high as 1800°C [18]. If the efficiency of SPS allow for such a lowering of the sintering temperature for refractory materials, it becomes tempting to also envision a significant efficiency of SPS at low temperature (typically $T < 700^\circ\text{C}$), for the sintering of a fragile materials such as MnSO_4 depicted above. At such low temperatures, the application of larger pressures may become necessary, to maintain the efficiency of SPS densification. Indeed, we recently reported [19] how Cool-SPS emerges as an original and powerful method for the sintering of

thermodynamically fragile materials at low temperature. The present work brings further experimental proofs to support this concept, while also offering some insight on the sintering mechanism at work during the densification of MnSO_4 by Cool-SPS. Through the evaluation of several experimental parameters, we aim at establishing a reproducible sintering route for the elaboration of dense (>90% compactness) MnSO_4 pellets. The role of the *in situ* dehydration and the transition to the high temperature form in the sintering mechanism will be investigated. Ultimately, dielectric characterizations enabled by the disposal of dense ceramics will allow to evaluate the potential multiferroic/magnetoelectric properties of MnSO_4 .

2. Experimental

Commercial $\text{MnSO}_4 \cdot \text{H}_2\text{O}$ powders were used (Sigma Aldrich 99.9% purity). Dehydration has been performed through two different ways, either through heat treatment in an oven under air for 24h at 300 °C, or during SPS processing. Spark plasma sintering (Dr. Sinter Lab spark plasma sintering system, Model SPS-511S/SPS-515S) experiments were performed with WC:Co 10 mm die using 0.5 g of powder for each sintering attempt. Temperature was controlled by a thermocouple in contact with the inner part of the die. The pulse sequence for the SPS applied voltage for all the samples was 12 ON/2 OFF. The densification was continuously monitored by the displacement of a punch rod. Heating rate was kept constant over the different sintering experiments and was set to 50 °C/min, while temperature and uniaxial pressure were varied from 400 °C to 600 °C and from 40 to 500 MPa respectively. Sintering attempts were performed under primary vacuum of about 10 Pa. Powder and pellet diffraction were performed with a Phillips X'Pert MPD X-ray diffractometer with the Bragg–Brentano geometry using $\text{Cu K}\alpha_1/\text{K}\alpha_2$ radiation ($10^\circ < 2\theta < 80^\circ$ range, step of 0.017°). The ceramics' relative densities were evaluated by geometrical measurements considering a theoretical density of 3.46 g/cm^3 for MnSO_4 [20] and 2.94 g/cm^3 for $\text{MnSO}_4 \cdot \text{H}_2\text{O}$ [21]. The pellets' microstructures were observed on fracture surfaces, with a scanning electron microscope (JEOL 840 SEM). TGA measurements were performed with a Setaram tag2400 apparatus coupled to a Balzer ThermoStar mass spectrometer. DSC datasets were collected with a Perkin Elmer DSC8000. Magnetic measurements were performed with a Quantum Design MPMS-5 (S.Q.U.I.D) magnetometer on powder and ceramics. Zero-field cooled and field cooled data were collected with an applied field of 1 kOe and with increasing temperature from 2K to 300K. Silver electrodes were deposited on both surfaces of the pellets and silver wires were subsequently used for sake of electrical connection. Once prepared for dielectric measurements, the ceramics were placed in a Quantum Design Physical Properties Measurement System (PPMS) from which a 9 T magnetic field can be applied. The dielectric measurements were carried out in the frequency range of 10^2 – 10^6 kHz (the amplitude of the applied

ac electric field being 1V) using an HP4194a impedance bridge, at heating and cooling rates between 0.2 and 1 K/min. Measurements of capacitance and dielectric losses were first performed by scanning temperature with and without application of a magnetic field of 9T. In a second step, the magnetic field was swept from -9T to 9T at 2K to evaluate magnetoelectric behavior of the samples. No dielectric dispersion was observed in the investigated frequency range, for all 8 various measured samples, thus a single frequency of 300 kHz is presented in the following.

3. Results and discussion

3.1 Phase stability

MnSO₄ phase in ambient conditions is only stable under hydrated form. The one used here is a monohydrated phase MnSO₄·H₂O (Hyd-MnSO₄) crystallizing in the monoclinic *A2/a* space group (n°15). It can be dehydrated at 300°C to form the anhydrous MnSO₄ (Anh-MnSO₄), which crystallizes in the orthorhombic *Cmcm* space group (n°63) corresponding to the α form, and transitions to the β form around 400°C [22] (in the following, the α form will be referred to as Anh-MnSO₄, and the β form as β -MnSO₄). The β form crystallizes in the space group *Pbnm* (n°62) and corresponds to a 45° rotation of oxygen octahedra around (001) axis. After dehydration, when the powder is put in ambient conditions, rehydration takes place within one or two days. Thus, for experiments performed on Anh-MnSO₄, powders and pellets were kept in an oven (at 120 °C) after thermal treatment and directly placed in the SPS die (for sintering) or the measurement setup (for characterization of the pellets). This way, the average ambient air exposure does not exceed 10-20min, and the sample is considered anhydrous. The two phases Hyd-MnSO₄ and Anh-MnSO₄ were both used for sintering experiments and compared.

3.2 Preliminary exploration of sintering conditions

Multiple sintering attempts have been performed under different experimental conditions. Selected parameters were temperature, time, pressure, and the use of anhydrous or hydrated precursor, which will be discussed in the following. Figure 1 summarizes some selected samples sintering conditions and densification results.

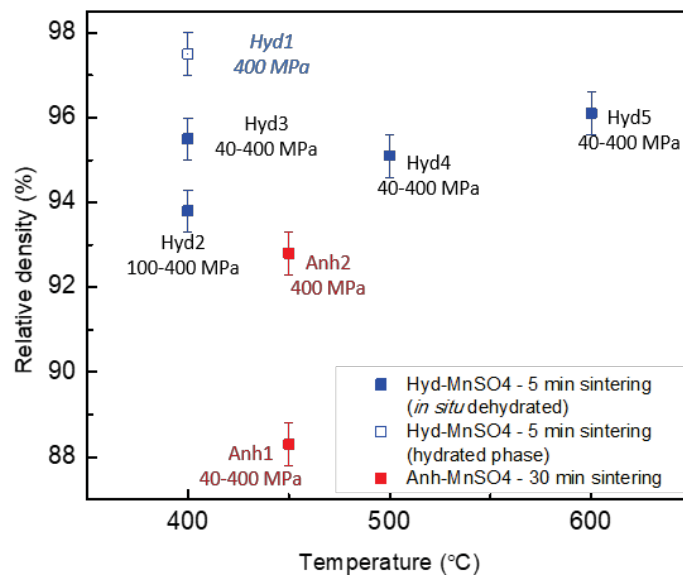


Figure 1: Densification results after SPS sintering of hydrated (hyd) and anhydrous (anh) precursors in various conditions of temperature and pressure. Anhydrous samples sintering had to be extended to 30 min to obtain cohesive ceramics. For some samples, two pressures are indicated, corresponding to pre-dwell pressure and dwell pressure respectively, detailed in section 3.2.2.

In this figure, to some samples are assigned 2 different pressures. The first pressure corresponds to the applied pressure during heating ramp, while the second one corresponds to the pressure applied during dwell time. This specific protocol will be described in detail in section 3.2.2. The first observation from Figure 1 is that all the presented samples, except Anh1, show a high density above 90 %, for sintering temperature down to 400 °C. It is the first report on the sintering of MnSO₄, which decomposition occurs at 780 °C. Secondly, one can notice that the final compactness is higher when starting from Hyd-MnSO₄ than from Anh-MnSO₄. Moreover, it was necessary to increase both temperature and time to 450 °C and 30 min respectively to obtain dense samples from anhydrous precursors. This suggests that structural water is involved in the sintering process. In the case of Hyd1, dehydration did not occur, therefore the hydrated form is preserved after sintering, and the resulting pellet displays a density close to 98% which is remarkable. This observation points out the importance of temperature-pressure profile, which will be detailed in section 3.2.2.

3.2.1 - Role of hydration

TGA measurement of Hyd-MnSO₄ raw powder and of Anh-MnSO₄ pellet (Hyd3, sintered at 400 °C) are displayed on Figure 2. The hydrated powder loses 10.8 wt.%, which is expected from the dehydration of MnSO₄·H₂O, while the pellet contains about 0.5 wt.%, corresponding to a composition of MnSO₄·0.04H₂O. This residual water likely results from the adsorption of water, or partial rehydration, that occurred between pellet removal from the die and the beginning of TGA measurement (*i.e.* in a span of 30 min in total). This confirms efficiency of the *in situ* dehydration during Cool-SPS treatment

at 400 °C, and suggests a form a reactive sintering, the water lost during the sintering being structural, and thus bonded to other constituting species in the precursor powder $\text{MnSO}_4 \cdot \text{H}_2\text{O}$.

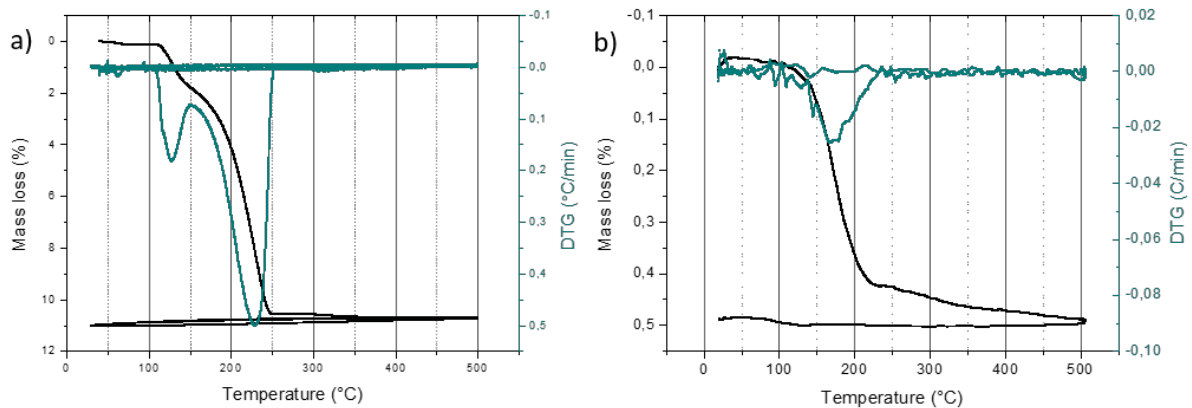


Figure 2: TGA measurement under air at 3 K/min of a) Hyd-MnSO₄ powder and b) Hyd3 pellet sintered at 400 °C under 40-400 MPa

Indeed, when using dehydrated powders, no pellet can be obtained below 450 °C, and a 30 min dwell time is needed anyway, whereas for hydrated powders, sintering at 400 °C for 5 min is enough to reach densification above 90 % (cf Figure 1). Similar conclusions have recently been drawn for cold sintering process and hydrothermal sintering [23][24], especially in the case of ZnO [25], which can also be processed by SPS at 400 °C when water is added to the powder [26,27]. However, in the case of ZnO, the optimal content of water added for sintering has been determined to be 1.7 wt.% and increasing it, even to 7.7 wt.%, strongly hinders densification. Recent study on flash sintering of ZnO powder with addition of water also confirmed these observations [28]. In the present case, water content represents 10.8 wt.% which is far above the optimal content determined for ZnO, although it consists exclusively in structural water, as no water is added to the Hyd-MnSO₄ powder. Moreover, water is released specifically during *in situ* dehydration in the present study, while added water is lost continuously during the processing in the afore-mentioned examples on ZnO. This suggests that there is an added value to the use of hydrated precursors, in Cool-SPS but also likely in alternative water assisted sintering methods. Indeed, being able to control the release of water, as in the present work, allows for further optimization of the experimental conditions and, ultimately, for a better densification. Thus, the present results show that a water-assisted sintering mechanism can be triggered in SPS conditions without water addition, by the simple use of hydrated precursors and the control of *in situ* dehydration. This constitutes a valuable processing commodity allowing for simpler and easier processing protocols.

3.2.2. Pre-dwell pressure application

Most of the time, thermal and mechanical pressure profiles are as follows: pressure is applied first on the powder while room temperature is maintained, then temperature is raised once the targeted pressure is reached. Dwell time starts when temperature reaches its maximum. After dwell time is over, temperature and pressure are both released (Figure 3 a). In several of the experiments presented in this paper, temperature is raised first while a pre-dwell pressure is applied. Due to the use of a 10 mm diameter die, and the application of a minimal force of 3kN to ensure electrical contact, this pre-dwell pressure is at least 40 MPa. Thus, this pre-dwell pressure can vary within the range $40 \text{ MPa} < P_{\text{pre-dwell}} < P_{\text{dwell}}$. Once the dwell temperature is reached, the mechanical pressure is raised, and dwell time starts when the applied pressure reaches dwell pressure (Figure 3 b).

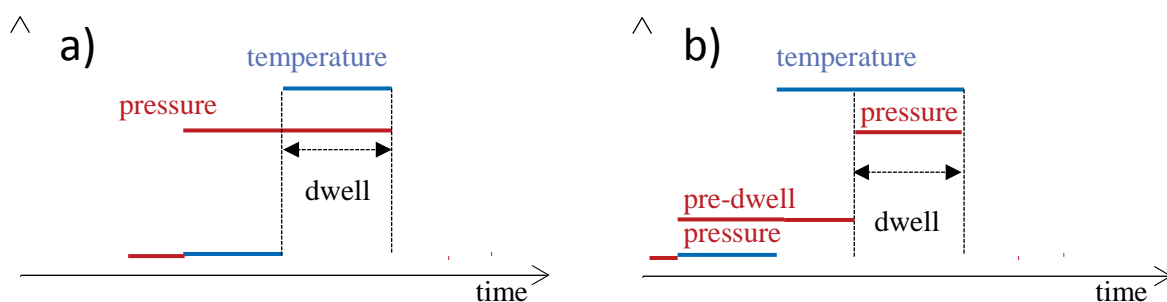


Figure 3: Schematic view of the two different strategies of SPS treatment. In the first case (a) pressure is set first and temperature increases when pressure is stable. In the second case (b), pressure is set lower pressure of the machine (>40 MPa) during heating. Once the temperature is stable at dwell value, pressure can be applied

In the case of Anh-MnSO₄ samples Anh1 and Anh2, introduction of a pre-dwell pressure of 40 MPa has a negative impact on the final density of the pellet, which is limited to 88.3(3) % (Anh1), while a relative density of 92,8(3) % (Anh2) is obtained when applying 400 MPa through the whole thermal cycle. This shows a strong influence of the pre-dwell pressure, especially when one considers that the sample Anh1 was maintained for a longer period at the dwell temperature (*i.e.* the time needed to increase pressure from 40 to 400 MPa is not considered as dwell time, although the dwell temperature of 450 °C is applied). In this case, it means that even if the total sintering time was longer for Anh1 than for Anh2, the latter sample is better densified. Interestingly, results from Hyd-MnSO₄ powders show the opposite behavior.

Among the three samples sintered from hydrated powder (Hyd1, Hyd2 and Hyd3) at 400 °C with different pre-dwell pressure, Hyd1 lead to hydrated structure whereas Hyd2 and Hyd3 where dehydrated *in situ*. Hyd2, with a pre-dwell pressure of 100 MPa, shows a density of 93.8(3), while Hyd3 sample, on which 40 MPa pre-dwell was used, reached 95.5(3) % relative density (*i.e.* an extra 1.6 %). During SPS experiments on Hyd-MnSO₄ powders, an increase of the gas pressure in the chamber, which is maintained under dynamic vacuum, was observed, signaling the release of gaseous species. Since subsequent characterization of the pellets excluded decomposition of manganese sulfate, it is

safe to associate this gas release to the *in situ* dehydration of the precursor powder. To highlight the influence of pre-dwell pressure, specific experiments were conducted that are summarized in Figure 4. Figure 4 a) displays the SPS chamber pressure during heating for Hyd-MnSO₄ samples under various pressures (maintained constant throughout the whole SPS processing). Although the heating ramp and atmosphere of TGA are different from that used during SPS (3 °C/min under air vs. 30 °C/min under vacuum, respectively), TGA under air is also displayed as a pressureless reference concerning dehydration temperature, for a qualitative comparison. With increasing mechanical pressure, dehydration is shifted to higher temperatures, and this phenomenon already occurs under a pressure of 40 MPa. At this stage, a single maximum of water release is located at 290 °C, which is 60 °C above the maximum of water release observed in TGA, and the dehydration apparently occurs in a single broad step, instead of 2 steps in TGA conditions. When the pressure is raised up to 100 MPa, dehydration again occurs in two steps, and the temperature of the maximum water release increases. At 300 MPa, the two main peaks at 350 and 380 °C differ in their amplitude, the first one being slightly more intense than the second one. When sintering is performed under a pressure of 300 MPa, the two peaks are again moved to higher temperatures, respectively ~370 and 415 °C (the location of this second peak being difficult to determine due to gauge saturation), and the latter one is now the more intense; *i.e.* the major part of dehydration is moved to higher temperature. It is noteworthy also that dehydration is barely completed at 400°C under 100 MPa, while for higher pressures it is necessary to go beyond 400 °C for dehydration to be complete. Thus, the sequence in which the thermal and pressure cycles are applied has an impact on the dehydration temperature, which increases with pressure. Moreover, the span of temperature within which this dehydration occurs narrows with increasing pressure. On one hand, this explains the observation on Figure 4b, displaying XRD patterns for Hyd1, Hyd2 and Hyd3, of the preservation of the hydrated phase in the case of a 400°C dwell temperature and 400 MPa pre-dwell pressure, the latter forbidding the dehydration before or at the dwell temperature. On the other, in the cases in which dehydration occurred (100 and 40 MPa), the final phase is Anh-MnSO₄. One can observe the incomplete dehydration of the sample sintered at 100-400 MPa on Figure 4, for which both chamber pressure (a) and XRD (b) are displayed.

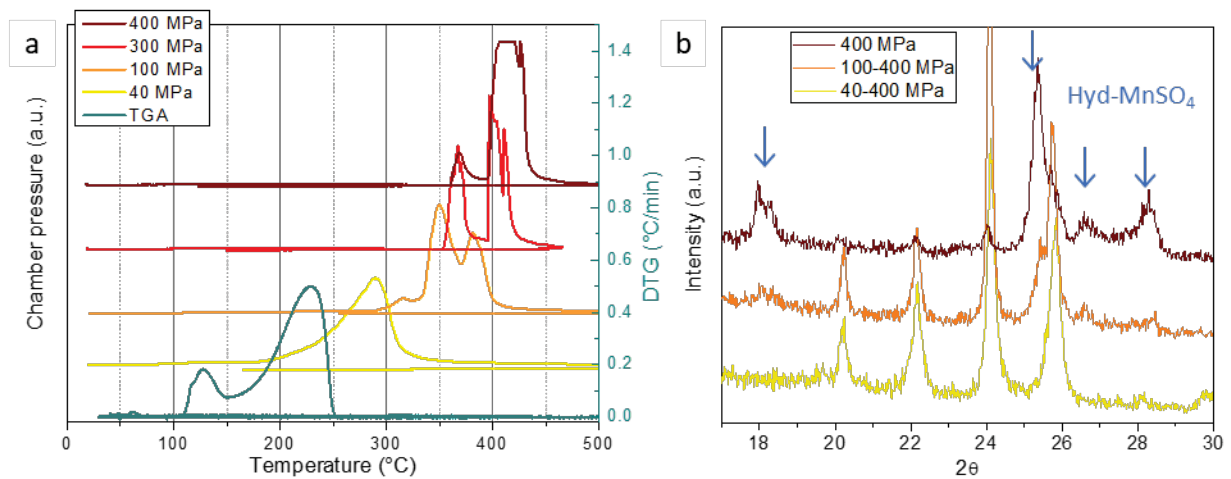


Figure 4: a) Chamber pressure during SPS experiment on $\text{MnSO}_4 \cdot \text{H}_2\text{O}$ for various applied pressures; TGA under air in atmospheric pressure is used as reference. b) XRD patterns of Hyd1, Hyd2, Hyd3 corresponding to pre-dwell pressures of 400, 100 and 40 MPa. Blue arrows highlight the presence of $\text{MnSO}_4 \cdot \text{H}_2\text{O}$ phase in 100-400 and 400 pellets.

These observations confirm the possibility to control dehydration through pressure monitoring. In the present case, the starting powders always contain 10 wt. % of (structural) water, and densification is enhanced when dehydration is completed in situ, the final Anh- MnSO_4 samples encompassing less than 0.05 wt.% of water (see Figure 2). This proves the presence of a different sintering mechanism, driven (partially at least) by dehydration. Results obtained on Hyd1 demonstrates the possibility to obtain a dense ceramic from a hydrated phase, thus confirming the presence of additional sintering mechanism, or of a combination of different mechanisms.

3.2.3. Dwell temperature and pressure

Various pressures have been explored to identify a range in which the densification could be enhanced without exceeding upper limits above which the mechanical cohesion is put in jeopardy. A few of them is sufficient to explain the influence of pressure on the sintering and are presented in Figure 5. Temperature also has been tested to evaluate its influence on sintering. The most significant results of this survey are summarized in the same figure.

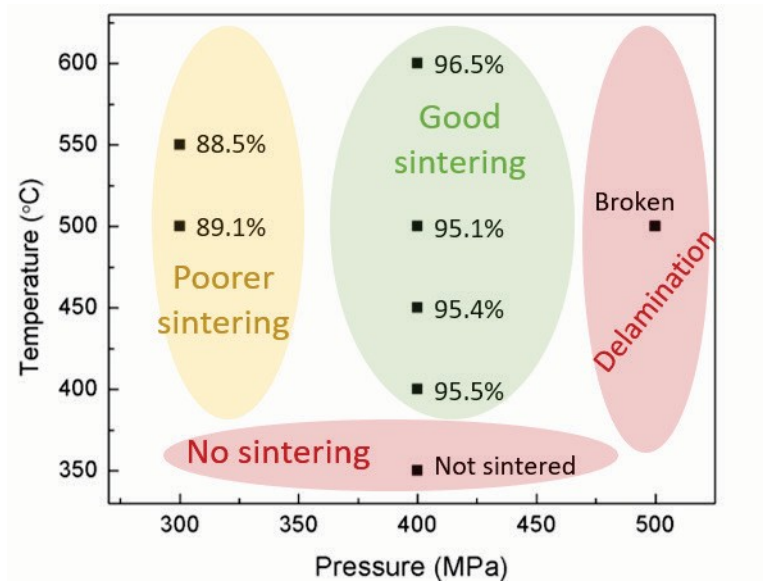


Figure 5: Densification level obtained for various sintering temperature and pressure conditions. All samples were sintered from a $MnSO_4 \cdot H_2O$ powder, during a soaking time of 5 min, and a pre-dwell pressure of 40 MPa was applied before the sintering pressure was set

In these experiments, for the same temperature (500 °C) and time conditions (5' dwell time), but also same powder quantity, the only difference is the different pressures applied during sintering. From 300 to 400 MPa, the density increases from 89 % to 95 % of theoretical density. When the pressure reached 500 MPa, the resulting pellet broke down during pellet's manipulation by delamination, which is indicative of an excessive applied pressure. These results have been reproduced on several occasions. As a general result, we never reached 90 % density for pellets sintered at 300 MPa, even for higher temperatures and longer dwell times. Therefore, not only pressure plays a role during the dehydration step, but also has a huge impact on densification during dwell, with a necessity to apply an important load of 400 MPa. Pressure has a complex impact on densification mechanisms, promoting rearrangement in the early sintering stages, enhancing plastic deformation, and increasing solid-solid surface tensions, possibly resulting in higher solid-state diffusion through grain boundaries. Surprisingly, no improvement of relative density is observed from 400 (95.5%) to 500°C (95.1%), and only 1.5 % difference between 500 and 600 °C (96.6%).

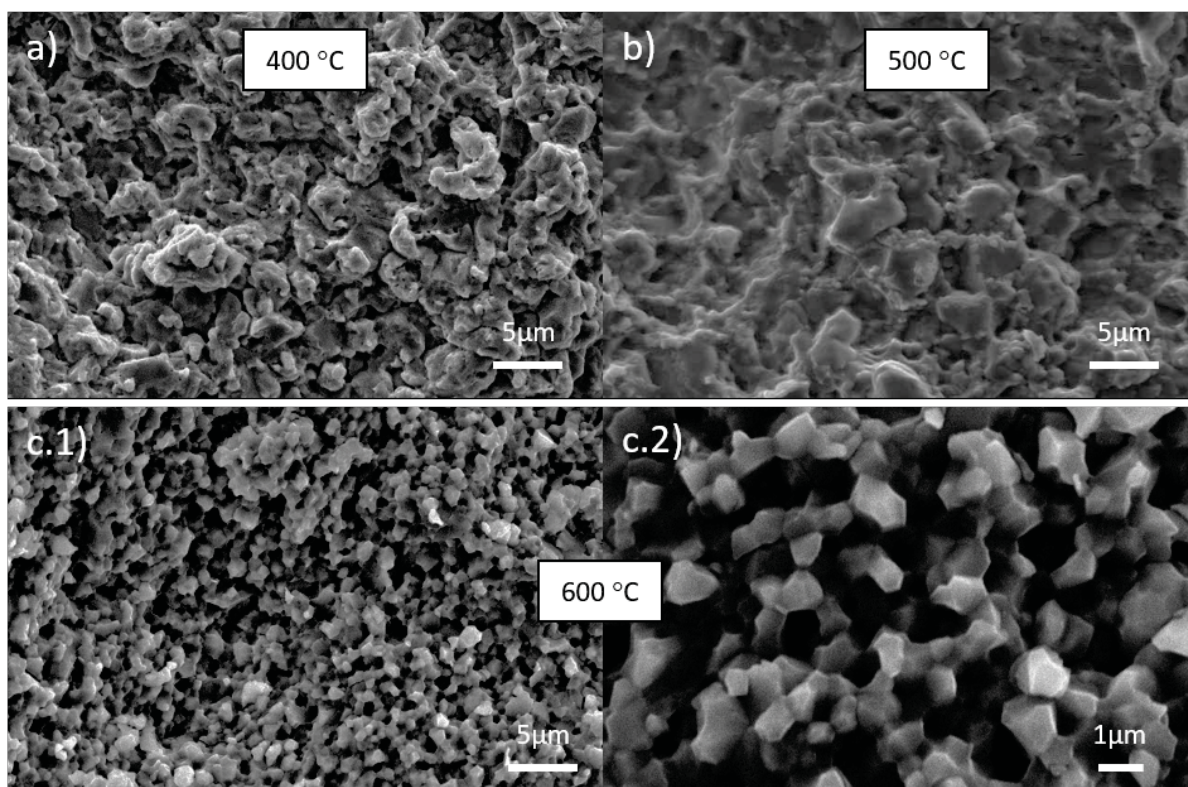


Figure 6: SEM images of $MnSO_4$ pellets sintered at (a) 400 °C, (b) 500 °C and (c.1 & c.2) 600 °C

On figure 6 are displayed SEM images of the fractures of three different pellets sintered at different temperatures. The observation of grain shape shows that samples sintered at 400 and 500 °C have similar size and shape, although some faceting seems to occur at 500°C. However, these two samples present the same compact microstructure, while the one sintered at 600 °C looks different. The first two are composed of grains of about 3-5 μm, with curved shapes, whereas the last one looks to be composed of small grains of about 1 μm with nice facets. This observation is in line with the relative density increase and suggests that a process (diffusion in the solid state, grain growth...) is triggered between 500 and 600 °C that induces a density increase and a change in the grains shape.

3.2.4 α - β Phase transition

At ambient temperature, Anh- $MnSO_4$ crystallizes in the $Cmcm$ space group ($n^{\circ}63$), and this form is called α - $MnSO_4$ (but Anh- $MnSO_4$ throughout the manuscript). It undergoes a reversible transition to a β phase at 380 °C under Ar and reverts to the α phase at 150 °C on cooling (Figure 7a). On Figure 7b is represented the temperature of maximum dehydration as detected by monitoring the gas pressure in the SPS chamber, with respect to the mechanical pressure applied on the sample (from Figure 4). The first point at 0 MPa corresponds to the dehydration measured from TGA, used as a reference. After a first increase of the pressure to 40 MPa, a 20 °C increase of the maximal water release temperature is observed. This can be explained by the application of pressure on the sample that slightly stabilizes

the monohydrate form. The evolution of dehydration temperature under pressures ranging from 100 to 400 MPa shows a different scheme, as it seemingly reaches a plateau at 100 MPa, and after this point, remains essentially constant (it should be reminded here that the dehydration typically takes place over a 20-30° range at the least). The red ribbon, with a width of about 50°C, represents the temperature range in which the phase transition from α to β form takes place, as extracted from the DSC measurement represented on Figure 7a. At about the same temperature (380 °C), we demonstrated that the dehydration of the powder (under 40-400 MPa) and its sintering occur. When larger pre-dwell pressures are applied, the dehydration still occurs around 400°C. The unique range of temperature in which both dehydration/sintering and phase transition take place raises the question of the involvement of the α - β phase transition in the sintering mechanism, and particularly as a triggering event for dehydration, which is itself critical to the sintering as illustrated earlier. It has been discussed elsewhere that phase transitions taking place during the sintering process can have an impact on the resulting densification [29]. It appears that fast dehydration, associated to phase transition, imply an important stress on the grains, which is even assisted by an external mechanical pressure during sintering, and results in the onset of sintering. Moreover, the applied pressure may influence the stabilization of either α or β phases, depending on their respective density. However, literature data for β phase are given for a temperature of 450 °C, whereas for α phase, density is given at room temperature. *In situ* XRD measurement has been performed on MnSO_4 powder at room temperature and at 350 °C, both showing a pure α phase. Lattice parameters refinements for these two patterns lead to lattice volume evolution from 288.54(1) Å³ to 295.51(1) Å³ for 25 and 350 °C respectively. Linear extrapolation of these values can give a hypothetical cell volume at 450 °C for the α phase which would be 298 Å³, which would result in a density of 3.37 g/cm³ at 450 °C. Considering the density of β phase at the same temperature, being 3.35 g/cm³, it means α phase would be 0.6 % more dense, therefore, the application of external mechanical pressure on the sample may slightly favor its stabilization. However, considering this small density variation, and the variation of applied pressure (from 40 to 400 MPa at dwell temperature) on one hand, it is difficult to formally affirm that pressure has an influence on the α - β phase transition. On the other hand, considering the dependence of the dehydration temperature on applied pressure, and the plateau it reaches in the region of the α - β phase transition, it is likely that this transition triggers the dehydration.

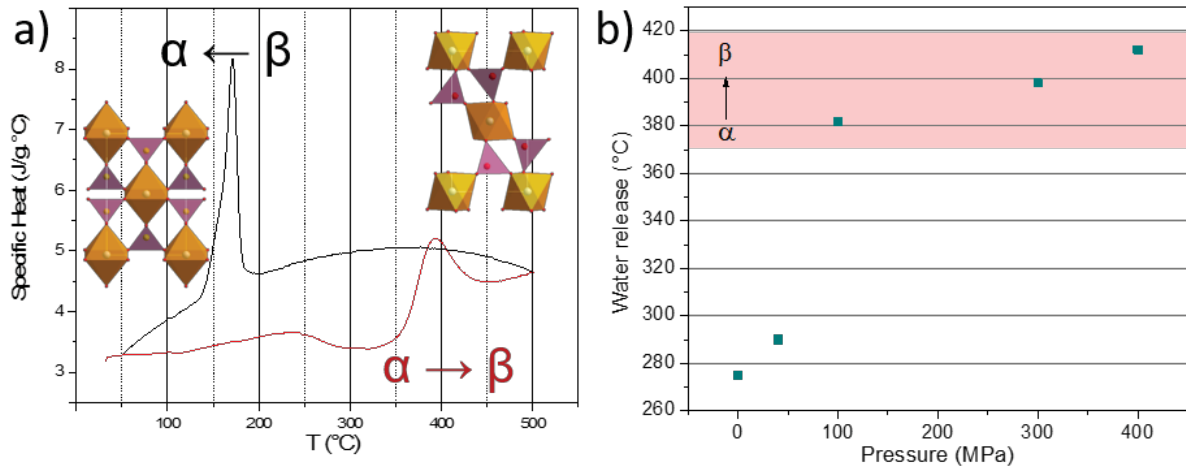


Figure 7: a) DSC measurement of Anh-MnSO₄ powder under Ar at 10K/min, the peak below 300 °C corresponds to adsorbed water release (inset correspond to α and β structure view along (001) direction; b) Green dots represent the temperature of maximal water release during SPS sintering and red box represents the temperature range of α to β phase transition in ambient pressure. Data at 0 MPa is extracted from TGA.

3.2.5 – Sintering mechanism

Beyond the previous observations, no formal proof of the influence of the phase transition can be collected in our experimental conditions, since it is impossible to prove the presence of the β phase during SPS processing. Indeed, the α phase is restored at the end of the experiment, and no signature of the α-β transition could be detected from SPS monitoring data. Yet, based on the fact that dehydration and α-β phase transition (as well as sintering) occur in the same temperature range, it is difficult to exclude the α-β phase transition from consideration as no alternative explanation can be provided for the observed plateau of the dehydration temperature. One could thus consider that the dehydration observed at 400°C under pressure of 100 MPa and beyond, is actually forced by the transition to β-MnSO₄, a phase for which no hydrated form is known. In this case, the role of this phase transition, and that of the dehydration, could be interwoven in the sintering mechanism. Therefore, the question is to know whether the role of the α-β phase transition is

- a direct one, in which sintering occurs thanks to the transition
- an indirect one, if this transition triggers the dehydration that allows for the sintering

The results obtained on Anh-MnSO₄ clearly exclude the first option, as relying solely on the α-β transition does not allow to obtain highly dense ceramics at 400°C.

The results obtained on Hyd-MnSO₄ at 350°C also exclude the second option, as relying solely on dehydration does not allow to obtain cohesive, mechanically strong pellets.

As a consequence, we propose that the sintering mechanism for MnSO_4 actually involves a coupling of the α - β transition and the dehydration, in which:

- dehydration allows for a very efficient densification (*i.e.* increase of relative density)
- dehydration is triggered by the α - β phase transition
- α - β transition and coupled dehydration allows for a simultaneous and efficient densification and consolidation (*i.e.* good cohesiveness of the final ceramic, intergranular bonding)

Indeed, considering the efficient densification provided by dehydration, the volume per formula unit of Hyd- MnSO_4 is 95.3 \AA^3 , while that of Anh- MnSO_4 is 72.7 \AA^3 . This represents a diminution of 23% of the volume per formula unit that likely accounts significantly for the densification associated to dehydration. Moreover, as highlighted above, it is difficult to justify the plateau of the dehydration temperature without consideration of the α - β phase transition. Finally, when relying on conditions allowing only for dehydration or α - β phase transition, no efficient sintering can be obtained. Thus, such a mechanism is fully consistent with all our experimental observations, and especially with the characteristics of pellets sintered in optimal conditions (Hyd- MnSO_4 , 40-400 MPa, 400°C), which are perfectly anhydrous and single phase, very cohesive (as experienced when breaking the pellets to investigate fracture surfaces) and highly densified.

3.3. Characterization

3.3.1. Magnetic characterization

Although XRD clearly points towards the successful densification of α - MnSO_4 , magnetic measurements were nonetheless performed to confirm the conservation of the magnetic properties after SPS sintering. Figure 8a displays the magnetization of both the anhydrous powder and the corresponding SPS pellet (sample Hyd3 in Figure 1). Both exhibit the same response, although a slight decrease of magnetization between powder and pellet from 0.70 to 0.67 emu/g can be noted. The Neel temperature $T_N=11\text{K}$ corresponds to the reported magnetic transition of α - MnSO_4 [30] and no transition is visible at 16K, which is the Neel temperature of the $\text{MnSO}_4 \cdot \text{H}_2\text{O}$ phase [30]. This result further confirms the purity of the phase, and validates SPS as an effective route for the sintering of this thermodynamically fragile phase.

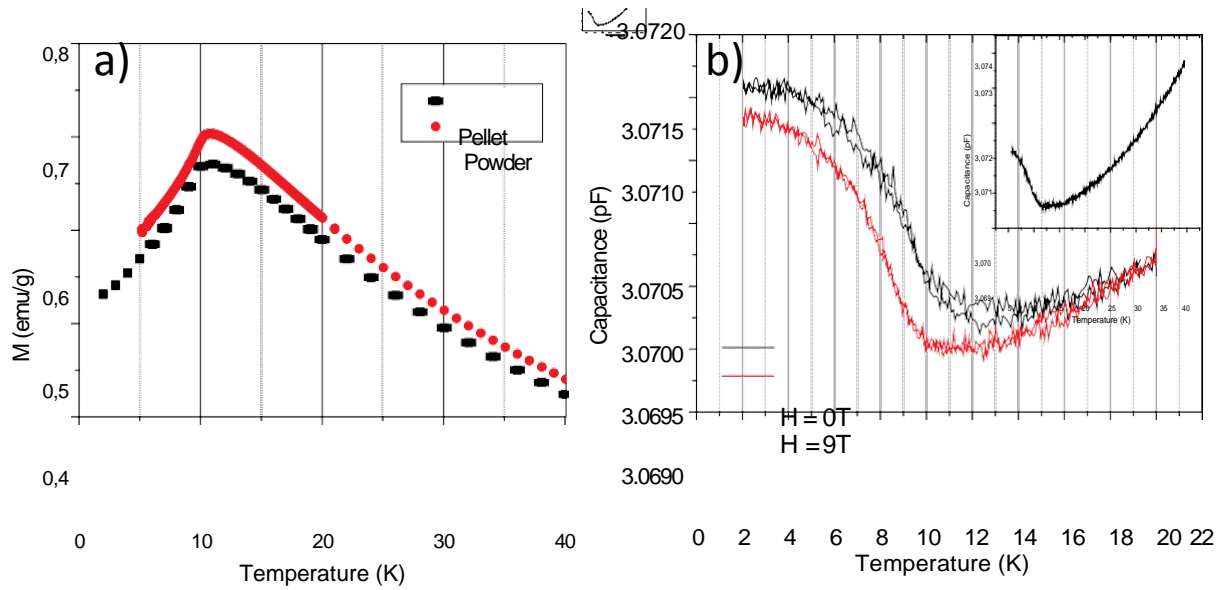


Figure 8: Temperature scan of a) magnetization under 1000 Oe in ZFC and b) capacitance measurement both while heating and cooling with and without magnetic field applied, at constant heating rate of 1 K/min and frequency measurement of 300 kHz. Inset represents scan without magnetic field on 2-300 K scale. Pellets made in the same conditions as Hyd3 (400 °C, 40-400 MPa, 5 min) have been used for these measurements.

3.3.2. Capacitance and magnetocapacitance characterization

Capacitance measurements were performed on several samples exhibiting relative densities higher than 90%. Figure 8b displays the thermal evolution of capacitance at 300kHz with (red curve) and without (black curve) magnetic field for Hyd3 sample (sintered 400 °C, 40-400 MPa). Whatever the magnetic field, a similar decrease of the capacitance from 300K to ca. 18-20K is observed, followed by an increase from 11K (*i.e.* T_N) down to 2K. This dielectric anomaly, being observed around T_N , can be considered as an intrinsic feature of α -MnSO₄, and this is further supported by the dielectric loss factor $\tan\delta$ (not displayed) that remains inferior to 0.05% up to 175K, thus ruling out extrinsic contributions such as those associated to defects or electrodes, for example. Upon application of a 9T magnetic field, the onset of this second signal is repelled to 10K, and the permittivity decreases ($\Delta\varepsilon'/\varepsilon'(\max) = 0,15$ %), claiming for an intrinsic magnetocapacitive coupling. Considering the helicoidal magnetic structure of α -MnSO₄, investigated both theoretically [31] and experimentally [20], these observations could be the signature of a type II multiferroic behaviour, with a dielectric anomaly associated with the antiferromagnetic transition and a magnetoelectric coupling related to the polarization possibly generated by this specific magnetic structure. However, the anomaly detected in the case of MnSO₄ cannot be directly ascribed to a ferroelectric transition (contrary to MnWO₄ [12]), although the transverse conical magnetic structure is indeed expected to induce a spontaneous polarization [32]. This discrepancy remains unexplained at present, but one should keep in mind that the magnetic structure model was (necessarily) built on a limited amount of data fifty years ago, and some subtleties hindering the onset of a polarization may have remained hidden. Nonetheless there is a clear connection between the onset of the antiferromagnetic state, the corresponding dielectric anomaly

and the magnetocapacitance effect observed that confirms the potential of α -MnSO₄ as a multiferroic/magnetolectric. To further characterize the magnetolectric behavior of α -MnSO₄, magnetic field dependent capacitance measurements were performed.

Isothermal magnetocapacitance measurements, performed by sweeping the magnetic field at 2K, are displayed on Figure 9. The capacitance presents a clear dependence on magnetic field, with different regimes. From 0 to \pm 2T the capacitance increases, while from (\pm) 7 to (\pm) 9T it decreases, but a more complex behaviour is found for magnetic field ranging from (\pm) 2 to (\pm) 7T. Indeed, a hysteretic dependence of the capacitance is observed in these conditions, and could be related to a magnetically induced polarization, possibly a ferroelectric phase induced by the applied magnetic field. This behaviour is confirmed on all the α -MnSO₄ ceramics measured (> 10 samples), and strongly supports the existence of a magnetolectric coupling.

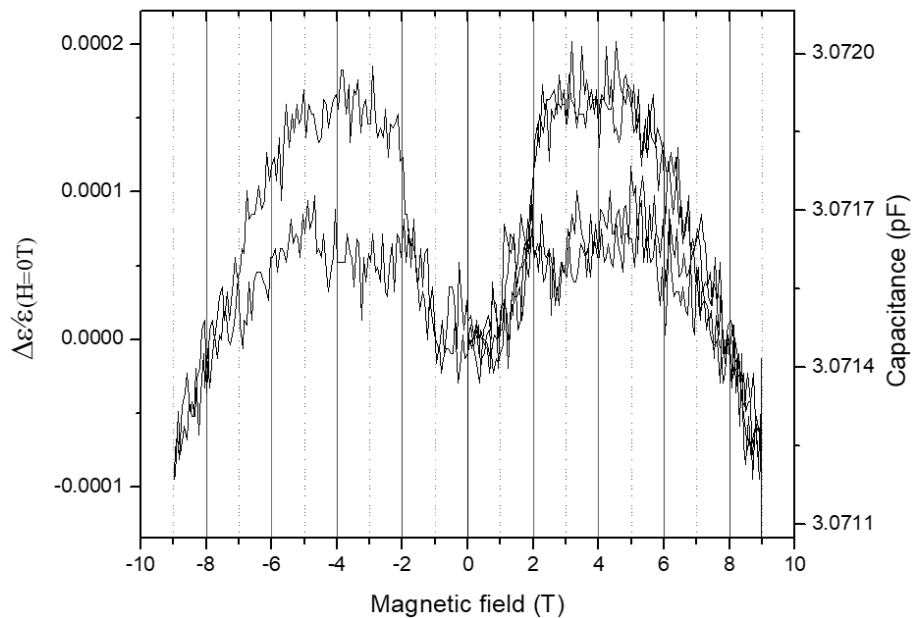


Figure 9: Magnetocapacitance measurement at 2K, 300 kHz. Pellet sintered at 400 °C, 40-400 MPa for 5 min was used for measurement. $\Delta\epsilon/\epsilon$ is calculated considering the ϵ at 0 zero magnetic field.

4. Conclusion

Cool-SPS was recently established as an efficient and reliable route to explore the ferroic properties of thermodynamically fragile materials in ceramic form [19]. The present work on α -MnSO₄ pushes further the proof of concept of this approach. This thermodynamically fragile material was successfully sintered, with relative densities up to 95.5 % while operating at 400°C. Investigation of various processing parameters highlights a complex sintering mechanism involving in situ dehydration and a reversible phase transition which are coupled, through adequate experimental conditions. Characterization of the processed ceramics confirmed the complete preservation of the structural and

physical-chemical properties of the parent (anhydrous) powder. Moreover, a highly dense ceramic of $\text{MnSO}_4 \cdot \text{H}_2\text{O}$ has been obtained (98 % theoretical density), which is, to our knowledge, the only example of ceramic made of a hydrated phase. The use of such hydrated precursor allows a better control over dehydration process and a highly homogeneous concentration of water over the sample compared to classical low temperature sintering processes involving the presence of added water. Beyond the successful processing of these ceramics, physical characterizations revealed a dielectric anomaly associated with the antiferromagnetic transition observed at 11K, a magnetocapacitive coupling, and a hysteretic behavior of the magnetocapacitance. This latter observation is associated to an abrupt modification of the capacitance for a magnetic field around 2T, which likely signals a transition induced by the magnetic field. All these observations point towards a probable magnetoelectric coupling and demonstrate that elaborated functional properties can be found in thermodynamically fragile materials, which are thus much worthy of further exploration. Ultimately, these results open a new route for the densification of thermodynamically fragile materials with potential multiferroic or magnetoelectric properties, and allow exploring known or new thermodynamically fragile phases for ferroic or other properties requiring ceramic samples.

- [1] N.A. Hill, Why are there so few magnetic ferroelectrics ?, *J. Phys. Chem. B.* 104 (2000) 6694–6709.
- [2] T. Kimura, T. Goto, H. Shintani, K. Ishizaka, T. Arima, Y. Tokura, Magnetic control of ferroelectric polarization., *Nature.* 426 (2003) 55–58.
- [3] N. Hur, S. Park, P.A. Sharma, J.S. Ahn, S. Guha, S.W. Cheong, Electric polarization reversal and memory in a multiferroic material induced by magnetic fields, *Nature.* 429 (2004) 392–395.
- [4] N. Spaldin, M. Fiebig, The Renaissance of magnetoelectric multiferroics, *Science* (80-.). 309 (2005) 391–392.
- [5] J.-W.G. Bos, C. V. Colin, T.T.M. Palstra, Magnetoelectric coupling in the cubic ferrimagnet Cu_2OSeO_3 , *Phys. Rev. B.* 78 (2008) 94416.
- [6] W. Bai, G. Chen, J.Y. Zhu, J. Yang, T. Lin, X.J. Meng, X.D. Tang, C.G. Duan, J.H. Chu, Dielectric responses and scaling behaviors in Aurivillius $\text{Bi}_6\text{Ti}_3\text{Fe}_2\text{O}_{18}$ multiferroic thin films, *Appl. Phys. Lett.* 100 (2012) 1–5.
- [7] C.E. Alarcon-Suesca, J.A. Cardona-Vasquez, J.P. Salcedo-Fontecha, A. Vargas-Jimenez, D.A. Landinez-Tellez, J. Roa-Rojas, Ferroelectric, magnetic and structural studies of the

- Bi₄LaSmFe₂Ti₃O₁₈ multiferroic material, *Phys. B Condens. Matter.* 455 (2014) 49–52.
- [8] R. Seshadri, N.A. Hill, Visualizing the role of Bi 6s “lone pairs” in the off-center distortion in ferromagnetic BiMnO₃, *Chem. Mater.* 13 (2001) 2892–2899.
- [9] T. Kimura, Spiral Magnets as Magnetoelectrics, *Annu. Rev. Mater. Res.* 37 (2007) 387–413.
- [10] Y. Tokura, S. Seki, Multiferroics with spiral spin orders, *Adv. Mater.* 22 (2010) 1554–1565.
- [11] D. Khomskii, Classifying multiferroics: Mechanisms and effects, *Physics (College. Park. Md.)* 2 (2009).
- [12] A.H. Arkenbout, T.T.M. Palstra, T. Siegrist, T. Kimura, Ferroelectricity in the cycloidal spiral magnetic phase of MnWO₄, *Phys. Rev. B - Condens. Matter Mater. Phys.* (2006).
- [13] T. Kimura, Y. Sekio, H. Nakamura, T. Siegrist, a P. Ramirez, Cupric oxide as an induced-multiferroic with high-TC., *Nat. Mater.* 7 (2008) 291–294.
- [14] V. Caignaert, A. Maignan, K. Singh, C. Simon, V. Pralong, B. Raveau, J.F. Mitchell, H. Zheng, A. Huq, L.C. Chapon, Gigantic magnetic-field-induced polarization and magnetoelectric coupling in a ferrimagnetic oxide CaBaCo₄O₇, *Phys. Rev. B - Condens. Matter Mater. Phys.* 88 (2013) 174403.
- [15] G. Will, B.C. Frazer, G. Shirane, D.E. Cox, P.J. Brown, Cycloidal Spin Configuration of Orthorhombic MnSO₄, *J. Appl. Phys.* 36 (1965) 1095.
- [16] P. Narayanchar, P. Basaveswara Rao, M. Aneesuddin, DTA studies on preparation of MnSO₄ by reacting pyrite and pyrolusite at high temperatures, *J. Therm. Anal.* 35 (1989) 1553–1560.
- [17] Z. Shen, M. Johnsson, Z. Zhao, M. Nygren, Spark Plasma Sintering of Alumina, *J. Am. Ceram. Soc.* 85 (2002) 1921–1927.
- [18] R.L. Coble, Sintering Alumina: Effect of Atmospheres, *J. Am. Ceram. Soc.* 45 (1962) 123–127.
- [19] T. Herisson de Beauvoir, A. Sangregorio, I. Cornu, C. Elissalde, M. Josse, Cool-SPS: an opportunity for low temperature sintering of thermodynamically fragile materials, *J. Mater. Chem. C.* (2018).
- [20] G. Will, The crystal structure of MnSO₄, *Acta Crystallogr.* 19 (1965) 854–857.
- [21] Y. le Fur, J. Coing-Boyot, G. Bassi, Structure des sulfates monohydrates, monocliniques, des metaux de transition, MSO₄ (H₂O) (M = Mn, Fe, Co, Ni et Zn), *Comptes Rendus Hebd. Des Seances l’Academie Des Sci. Ser. C, Sci. Chim.* 262 (1966) 632–635.

- [22] A. Kirfel, G. Will, New high temperature phase of MnSO_4 , *High Temp. - High Press.* 6 (1974) 525–527.
- [23] J. Guo, H. Guo, A.L. Baker, M.T. Lanagan, E.R. Kupp, G.L. Messing, C.A. Randall, Cold Sintering : A Paradigm Shift for Processing and Integration of Ceramics, *Angew. Chemie Commun.* 55 (2016) 1–6.
- [24] J. Guo, S.S. Berbano, H. Guo, A.L. Baker, M.T. Lanagan, C.A. Randall, Cold Sintering Process of Composites : Bridging the Processing Temperature Gap of Ceramic and Polymer Materials, *Adv. Funct. Mater.* 26 (2016) 1–7.
- [25] S. Funahashi, J. Guo, H. Guo, K. Wang, A.L. Baker, K. Shiratsuyu, C.A. Randall, Demonstration of the Cold Sintering Process Study for the Densification and Grain Growth of ZnO Ceramics, *J. Am. Ceram. Soc.* 6 (2016) 1–6.
- [26] B. Dargatz, J. Gonzalez-Julian, M. Bram, P. Jakes, A. Besmehn, L. Schade, R. Roder, C. Ronning, O. Guillon, FAST/SPS sintering of nanocrystalline zinc oxide-Part I: Enhanced densification and formation of hydrogen-related defects in presence of adsorbed water, *J. Eur. Ceram. Soc.* 36 (2016) 1207–1220.
- [27] B. Dargatz, J. Gonzalez-Julian, M. Bram, Y. Shinoda, F. Wakai, O. Guillon, FAST/SPS sintering of nanocrystalline zinc oxide-Part II: Abnormal grain growth, texture and grain anisotropy, *J. Eur. Ceram. Soc.* 36 (2016) 1221–1232.
- [28] J. Nie, Y. Zhang, J.M. Chan, R. Huang, J. Luo, Water-assisted flash sintering: Flashing ZnO at room temperature to achieve $\sim 98\%$ density in seconds, *Scr. Mater.* 142 (2018) 79–82.
- [29] C. Bousquet, C. Elissalde, C. Aymonier, M. Maglione, F. Cansell, J.M. Heintz, Tuning Al_2O_3 crystallinity under supercritical fluid conditions: Effect on sintering, *J. Eur. Ceram. Soc.* 28 (2008) 223–228.
- [30] Y. Allain, J.P. Krebs, J. De Gunzbourg, Magnetic study of the manganous sulfates MnSO_4 and $\text{MnSO}_4 \cdot \text{H}_2\text{O}$, *J. Appl. Phys.* 39 (1968) 1124–1125.
- [31] J. Solyom, On the theory of magnetic phase transitions I : Many-step phase transitions. Possible magnetic phase transitions in MnSO_4 , *Physica.* 32 (1966) 1243–1252.
- [32] Y. Tokura, S. Seki, N. Nagaosa, Multiferroics of spin origin, *Reports Prog. Phys.* 77 (2014) 76501.